

## Temperature Dependence of Hydrogen-Bond Stability in $\beta$ -Hairpin Structures

Qiang Shao and Yi Qin Gao\*

*College of Chemistry and Molecular Engineering, National Laboratory of Molecular Sciences, Peking University, Beijing, China*

Received August 6, 2010

**Abstract:** Understanding the temperature effect in the folding of multiple  $\beta$ -hairpins with different sequence (although based on an approximate solution model) makes possible quantitative characterization of the different contributing factors that are difficult to be obtained from single temperature studies. The detailed thermodynamics analyses performed in this article provide at least a semiquantitative understanding of how temperature and positions affect the stability of individual backbone hydrogen bonds in  $\beta$ -hairpin structures. These effects are then rationalized, according to the separation into enthalpic and entropic contributions. The formation of backbone hydrogen bonds at the terminal position is favored at low temperatures and those near the turn become more favorable at high temperatures, as a result of the differences in their formation entropy. Regardless of the differences in the turn stability, the side-chain hydrophobicity, and the room temperature folding mechanism of these  $\beta$ -hairpins, there is a shift to the “zip-out” mechanism in the assembling of backbone hydrogen bonds as temperature increases for all polypeptides under study. In addition, it was also observed that although the backbone hydrogen-bond formation shows a strong dependence on temperature, the formation order of the three structural elements of  $\beta$ -hairpin (the turn, hydrophobic core cluster, and hydrogen-bond assembly) along the minimum free energy pathway in the free energy landscapes appears to be only sequence dependent and largely unaffected by the temperature change.

### Introduction

As important model systems for protein folding,  $\beta$ -hairpin structured polypeptides have been the subject of a large number of experimental and theoretical studies.<sup>1–15</sup> The popular  $\beta$ -hairpins include not only fragments of natural proteins (e.g., those from the B1 domain of protein G (GB1 peptide),<sup>10,16</sup> ubiquitin,<sup>14</sup> and human chorionic gonadotropin)<sup>17</sup> but also artificially designed peptides (e.g., the tryptophan zipper series, TRPZIP 1–6).<sup>11</sup> Since the folding of  $\beta$ -hairpins is a cooperative process which largely resembles that of complex proteins,<sup>8,10</sup> the understanding of their folding mechanism and kinetics is of great interest. A great number of mechanistic studies have been performed, and different folding mechanisms have been proposed. These

mechanisms mainly differ in the arrangement of the important structural elements, such as the hydrophobic core cluster, the  $\beta$ -turn, and backbone hydrogen bonds. For instance, the laser-induced temperature-jump experiment<sup>10</sup> and the lattice Monte Carlo (MC) simulation<sup>18</sup> on the GB1 peptide suggested a “zipping” or “hydrogen-bond centric” mechanism. The folding of a  $\beta$ -hairpin starts from the turn and propagates to the terminus. During this process, the native backbone hydrogen bonds are formed. At the last stage, the hydrophobic core is packed. A modified version of the zipping model in which the hydrogen-bond formation instead of hydrophobic core packing occurs at last was also proposed based on molecular dynamics (MD) simulations on a GB1 peptide.<sup>19</sup> On the other hand, “hydrophobic core centric” mechanism as favored by several theoretical simulations<sup>4,20–24</sup> postulated that the hydrophobic core is packed first, during which a few backbone hydrogen bonds could also form. The

\* Corresponding author. E-mail: gaoyq@pku.edu.cn. Telephone: +86 010 62752431.

final stage of folding in this model consists of the formation of the remaining hydrogen bonds as well as the native turn structure.

These folding mechanisms of the  $\beta$ -hairpin are surmised based on the experimental observations and the simulation results. To date, many different all-atom force fields have been used for the computational simulations of  $\beta$ -hairpins, e.g., CHARMM, AMBER, OPLS, and GROMOS96, employed with either explicit or implicit solvent models. Different force fields favor different secondary structures, e.g., of the AMBER all-atom force fields, it is well-known that FF96 favors  $\beta$ -structures, whereas FF94, FF99, and FF03 favor  $\alpha$ -helical conformations.<sup>25–28</sup> On the other hand, the explicit solvent model is more desirable for elucidating the details of protein folding pathways at the cost of enormous CPU time, whereas the implicit solvent models are developed to economize the computation time with the loss of simulation precision. The most popular implicit solvent model is the generalized Born/surface area (GB/SA) model.<sup>29</sup> One of the potential sources for the inconsistency among these folding mechanisms mentioned above might be the usage of different force fields and solvent models in these simulations.

The question is: On the premise of saving the computation time, which force field and implicit solvent model should we use to best describe the folding pathway of  $\beta$ -hairpins? To answer this question, Zhou performed the replica exchange molecular dynamics (REMD) simulations on the folding of GB1 peptide with different force fields in combination with different implicit models and compared the results to those from explicit solvent models.<sup>30</sup> Of all implicit solvent models tested, only AMBER FF96/GBSA produced reasonable results comparable to the explicit solvent models.

More recently, Shell et al. tested the stability of several polypeptides (GB1 peptide, TRPZIP2, C peptide, and EK helix) with AMBER force fields and several versions of the GB/SA model.<sup>31</sup> It showed that the combination of FF96 with GB<sup>OBC</sup> model ( $igb=5$ )<sup>32</sup> is the best choice to balance the  $\alpha$ -helix and  $\beta$ -hairpin tendencies of the polypeptides tested. We also ran MD simulation on the folding of GB1 peptide using FF96 force field with both GB<sup>OBC</sup> and GBn ( $igb = 7$ )<sup>33</sup> models and compared the results to MD simulation using FF96 and TIP3P explicit solvent model.<sup>34</sup> The results showed that the combination of FF96 with GB<sup>OBC</sup> model generates the more consistent free energy landscapes compared to those in explicit solvent model and therefore is better at describing the folding of GB1 peptide.<sup>34</sup> Furthermore, Ozkan et al. ran the REMD simulations with the zipping and assembly (ZA) search strategy on the folding of nine proteins, including both  $\alpha$ - and  $\beta$ -secondary structures, and observed that FF96 force field, combined with GB/SA model, is best balanced for various secondary structures compared to other force fields.<sup>35</sup> All information mentioned above showed that although the combination of AMBER FF96 and GB<sup>OBC</sup> model might generate the folding thermodynamics data (such as folding/unfolding energy barriers) with the exact values inconsistent (not far away) with those in the explicit solvent simulation,<sup>30</sup> it is still good at depicting

the overall folding scene of  $\beta$ -hairpin. The latter is more interesting for us and is the main issue in the present study.

To distinguish between different folding mechanisms as mentioned above by quantifying the thermodynamics of the folding of  $\beta$ -structured polypeptides and, more importantly, to examine the sequence dependence in their folding mechanisms, in the recent study we ran MD simulations on the folding of a series of polypeptides using the integrated tempering sampling (ITS)<sup>36,37</sup> method and performed detailed folding thermodynamics analyses on these polypeptides at room temperature.<sup>38</sup> All polypeptides are modeled using the AMBER FF96 force field<sup>39</sup> and the GB<sup>OBC</sup> model,<sup>32</sup> the best force field and implicit solvent model combination. The advantage of this study is that the usage of the enhanced energy sampling method ITS allows the simulation to sample the potential energy surface thoroughly and thus to capture plenty of polypeptide configurations and, to some extent, reduces the influence of the force field and implicit solvent model.

It is worth noting that all theoretical models of  $\beta$ -hairpin folding mentioned above are based on the studies of a single system, GB1 peptide. A systematic study on the sequence influence of the folding mechanism of  $\beta$ -structures has not been carried out previously and therefore becomes very necessary. The systems in our study include peptide 1 (sequence: SESYIN<sup>D</sup>PDGTWTWTE),<sup>40</sup> GB1 (sequence: GEWTYDDATKTFTVTE, PDB code: 2GB1),<sup>41</sup> TRPZIP2 (sequence: SWTWENGKWTWK, PDB code: 1LE1),<sup>11</sup> and TRPZIP4 (sequence: GEWTWDDATKTWTWTE, PDB code: 1LE3).<sup>11</sup> The native structures of the four polypeptides are shown in Figure 1 (backbone hydrogen bonds (HBs 1–6) are named from the terminus to the turn positions in all polypeptides. For TRPZIP2, HB1 located at the terminus is not accounted in the data analysis due to its high instability). The sequence differences among these polypeptides are in their turn structure (either type I or type I') and side-chain hydrophobicity. TRPZIP2 and TRPZIP4 were designed based on the wild-type GB1 peptide with modified turn sequences and/or hydrophobic core cluster composition. Both of them exhibit reversible and highly cooperative thermal unfolding transition in solution.<sup>11</sup> The fourth hairpin, peptide 1, possesses a pair of very weak hydrophobic interactions but has a very stable (type I') turn.<sup>40,42</sup> Consequently, the folded peptide 1 and TRPZIP2 but not GB1 or TRPZIP4 possess stable turn structures. On the other hand, TRPZIP2 and TRPZIP4 possess very strong hydrophobic interactions, which are largely absent for GB1 and peptide 1.

Our folding free energy landscape calculations for the four polypeptides at room temperature showed that the folding mechanism of a  $\beta$ -hairpin is strongly dependent on its turn stability and side-chain hydrophobicity.<sup>38</sup> The stable turns of peptide 1 and TRPZIP2 make the turn formation a barrierless and spontaneous process in comparison with the formation of the hydrophobic core and backbone hydrogen bonds, while the turn formation in the other two polypeptides has to overcome significant free energy barriers and becomes the rate-limiting step in the hairpin folding process. Therefore, the turn stability is the key element in determining the formation order of the structural elements of a  $\beta$ -hairpin.

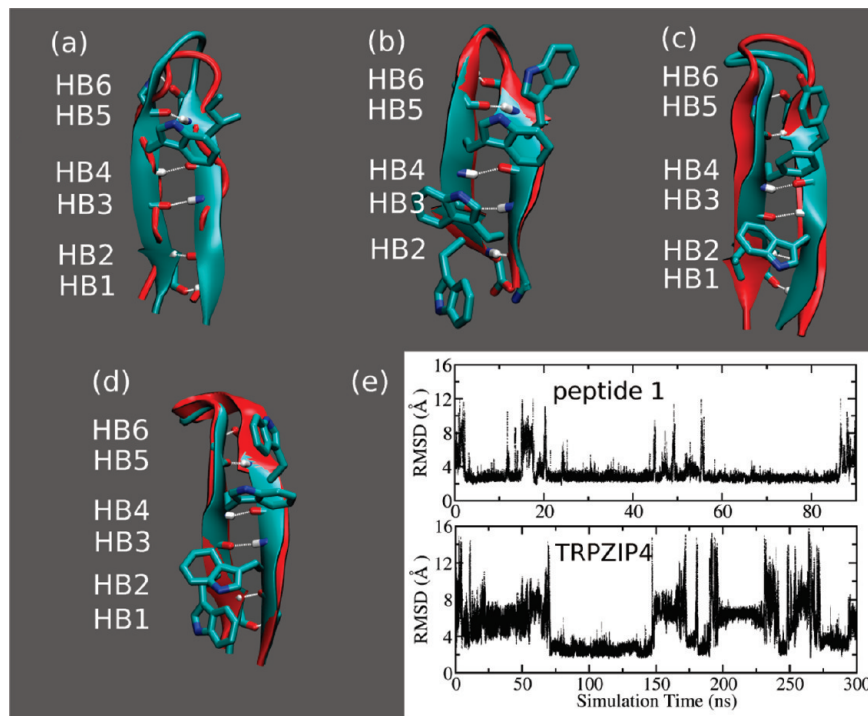


**Figure 1.** Folded structures of (a) peptide 1, (b) TRPZIP2, (c) GB1, and (d) TRPZIP4 polypeptides obtained in MD simulations (blue color) in comparison to their corresponding native structures (red color). The hydrophobic core is shown in licorice model, and backbone hydrogen bonds are represented by dash lines. (e) Time series of  $C_{\alpha}$ \_rmsd value in the typical trajectories of peptide and TRPZIP4.

This is perfectly consistent with the observation in the static IR and CD spectroscopy, and the IR temperature jump experiments by Gai and co-workers, which suggested that the turn plays a key role in the folding of  $\beta$ -hairpin; a strong turn-promoting sequence increases the stability of a  $\beta$ -hairpin by increasing its folding rates.<sup>43,44</sup> More interestingly, both turn structure and side-chain hydrophobicity were observed to strongly affect the backbone hydrogen-bond formation.<sup>38</sup> For instance, the stable turn of TRPZIP2 strongly promotes the formation of hydrogen bonds near the turn, and the hydrogen-bond formation follows a “zip-out” mechanism.<sup>45</sup> In contrast, the unstable turn of TRPZIP4 makes difficult the formation of the inner hydrogen bonds (HB5 and HB6). At the same time the strong hydrophobic interactions among the four tryptophan residues in TRPZIP4 allow the easy formation of the hydrogen bonds in the middle of the strands (H3 and H4), which is then followed by the zipping of the rest of the hydrogen bonds, both near the turn and the terminus.<sup>38</sup>

In this article, based on the folding simulation data obtained earlier<sup>38</sup> we performed detailed analyses on the temperature-dependent folding/unfolding thermodynamics for these polypeptides without explicitly considering the temperature effects in solvation, to understand in more detail the mechanisms of  $\beta$ -hairpin formation. We calculated the unfolding free energy of individual polypeptides and analyzed the stability of individual backbone hydrogen bonds in each polypeptide in a large temperature range (270–380 K). These detailed calculations allow us to determine important thermodynamic parameters, such as the melting temperature and the entropy and enthalpy changes in protein folding and in individual hydrogen-bond formation. As a

result of using the approximate solvation model (GB<sup>OBC</sup> model), as shown later, the calculated thermodynamics parameters, such as the melting temperatures, of all polypeptides are in rough agreement with experiments. Nevertheless, these results should be considered as qualitative; through these analyses, we could quantitatively distinguish the enthalpic and entropic contributions in the formation of native  $\beta$ -hairpin structures as well as individual backbone hydrogen bonds and thus try to understand quantitatively the sequence and the temperature dependence of hairpin formation.

It is worth noting that in a very recent article, Tokmakoff and co-workers reported their experimental observation of the temperature-dependent stability of the backbone hydrogen bonds of TRPZIP2 studied by isotope-edited two-dimensional infrared spectroscopy.<sup>46</sup> It was observed in this experiment that as temperature increases from 298 to 358 K, the turn region and its neighboring backbone hydrogen bond (HB6) become more stable, whereas the hydrogen bond at the terminus (HB2) is easily broken. The hydrogen bonds in the middle of the strands (HB3 and HB4) keep contacting at all temperature, whereas their thermal disorder is increased. This is in nice agreement with our simulation results for TRPZIP2 in the present study, which demonstrates that the methodology used here (AMBER FF96 combined with GB<sup>OBC</sup> implicit model and ITS sampling method) does provide reasonable qualitative descriptions of  $\beta$ -hairpin folding.

## Materials and Methods

All MD simulations were performed using AMBER 9.0 package. In the folding simulations of all polypeptides, GB<sup>OBC</sup> implicit solvent model<sup>32,34</sup> was used. The polypep-

tides were modeled with AMBER FF96 all-atom force field.<sup>39</sup> In these simulations, the salt concentration is set to 0.2 M, and the default surface tension is 0.005 kcal/mol/Å<sup>2</sup>. The SHAKE algorithm<sup>47</sup> with a relative geometric tolerance of 10<sup>-5</sup> is used to constrain all chemical bonds. No nonbonded cutoff was used in simulations. For each polypeptide, multiple independent trajectories were carried out for several hundred nanoseconds. In each trajectory, the fully extended structure of a polypeptide was first subjected to 2500 steps of minimization, then the temperature of the system was established by velocity rearrangement from a Maxwell–Boltzmann distribution at 300 K. After that the system was maintained at 300 K using the weak-coupling algorithm with a coupling constant of 0.5 ps<sup>-1</sup>. The ITS method<sup>36,48</sup> was used in the production run of each trajectory to enhance the energy sampling on the potential energy surface.

In the ITS method, a desired potential energy range corresponds to a temperature range in MD simulation. The temperature range could be separated into a series of smaller ranges, each having its own energy distribution. Using a quick and robust method, the ratio among the distributions in all small temperature ranges could be adjusted. As a result, the sampling in the entire energy (temperature) range becomes even.<sup>36,48</sup> Moreover, the energy range sampled in the ITS simulation could be largely extended. In the present study, 50 temperatures, evenly distributed in the range of 240–380 K, were used in the ITS method to ensure the efficient sampling of the desired energy range. In each trajectory, which was run at the constant simulation temperature, a large energy range was covered, and many folding and unfolding transitions were obtained.

**Backbone Hydrogen-Bond Definition.** A hydrogen bond is considered as formed only if the distance between the carbonyl oxygen and the amide hydrogen [C=O…NH] is less than 3.5 Å and the N–H–O angle is greater than 145°.

Heat capacity  $C_p$  was calculated by

$$C_p = (\langle E^2 \rangle - \langle E \rangle^2)/kT^2 \quad (1)$$

where  $E$  is the potential energy (the contribution of kinetic energy is treated as a constant and therefore is not taken into account in the calculation),  $k$  is the Boltzmann constant, and  $T$  is the temperature.

Unfolding free energy  $\Delta G_U$  of a polypeptide was calculated by

$$\Delta G_U = kT \ln \frac{P}{1-P} \quad (2)$$

where  $P$  is the formation probability of folded hairpin structures. The folded hairpins are defined as structures with at least three of backbone hydrogen bonds formed. This definition of folded hairpin structures is based on the characters of the folded states in the free energy landscape as a function of the radius of gyration of the hydrophobic core ( $R_g^{\text{core}}$ ) and the number of backbone hydrogen bond formed ( $N_{\text{HB}}$ ) ( $R_g^{\text{core}} < 5$  Å and  $N_{\text{HB}} \geq 3$ , see Figure 4a in ref 34, Figure 5 in ref 45, and Figure 2 in ref 38). The unfolding entropy and enthalpy were then calculated by  $\Delta S_U =$

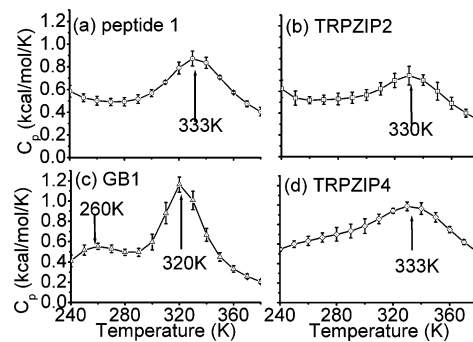


**Figure 2.** Temperature dependence of the heat capacity for four  $\beta$ -structured polypeptides.

$-(\partial \Delta G_U / \partial T)_P$  and  $\Delta H_U = \Delta G_U + T\Delta S_U$ , respectively. After we obtained the figure of  $\Delta G_U$  as a function of temperature ( $\Delta G_U$  vs  $T$ ), we assume that  $\Delta S_U$  ( $\Delta H_U$ ) is uniform in the time range of two neighboring temperature points ( $T_1$  and  $T_2$ ). Then  $\Delta S_U$  at that temperature range is equal to the slope of  $\Delta G_U$  vs  $T$ ,  $-(\Delta G_{U1} - \Delta G_{U2})/(T_1 - T_2)$ , and  $\Delta H_U$  is the intersection. For each polypeptide, all calculated trajectories in the simulation are involved in the calculation of  $C_p$ ,  $\Delta G_U$ ,  $\Delta S_U$ , and  $\Delta H_U$ . In the meanwhile, the corresponding thermodynamics parameters calculated from individual trajectories are used to generate error bars.

## Results and Discussion

**Temperature Dependence of the Folded Structure Stability.** For each polypeptide under study, more than 10 independent trajectories were run, each starting from the fully extended structure and lasting for several hundred nanoseconds. Consequently, the total simulation time is 1.0  $\mu$ s for peptide 1, 2.2  $\mu$ s for GB1, and 2.0  $\mu$ s for TRPZIP2 and TRPZIP4. Plenty of folding and unfolding events were observed for each polypeptide, e.g., totalling 57 folding events obtained for peptide 1, 19 for GB1, 24 for TRPZIP2, and 26 for TRPZIP4 (see the typical trajectories for peptide 1 and TRPZIP4 as examples in Figure 1). To investigate the conformational transition of the polypeptides, we first calculated their specific heat as a function of temperature in a large temperature range (240–380 K). Using the peak positions in their heat capacity diagrams as shown in Figure 2, we estimated the melting temperatures for the four polypeptides. As seen in this figure, the error bars are small for each polypeptide in the whole temperature range, which means that each trajectory in the simulation is well converged.

Except for the GB1 peptide, the experimentally determined melting temperatures for the four polypeptides are unarguable (e.g.,  $304.1 \pm 0.1$  K for peptide 1,<sup>40</sup>  $345.0 \pm 0.1$  K for TRPZIP2,<sup>11</sup> and  $343.1 \pm 0.1$  K for TRPZIP4).<sup>11,43,44</sup> The laser temperature jump experiment by Eaton and co-workers showed that the melting temperature of GB1 peptide is 297.3 K.<sup>10</sup> Nevertheless in the more recent NMR and CD spectroscopy experiments by Anderson and co-workers<sup>49,50</sup> and by Scholtz and co-workers,<sup>51</sup> the GB1 peptide demonstrated less stability in the aqueous solution with the determined melting temperature of 280–285 K or even lower to  $\sim 273$  K. The calculated heat capacity diagrams for the four polypeptides except GB1 show a single peak at  $\sim 330$  K,

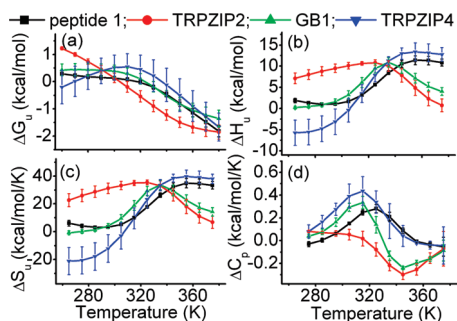


**Figure 3.** (a) Temperature dependence of the unfolding free energy, (b) enthalpy change, (c) entropy change, and (d) heat capacity change for four polypeptides.

while the diagram of GB1 shows a minor peak at 260 K in addition to the major peak at 320 K. The experimentally determined melting temperature of GB1 is in the middle of the two peaks. For the other three polypeptides, the calculated melting temperatures are about 15 °C too low for TRPZIP2 and TRPZIP4 but are ~20 °C too high for peptide 1 compared to the experimental data.

The usage of the current force field and the implicit solvent model is considered to be the potential source for the deviation between the calculated and experimental melting temperatures. As mentioned earlier, compared to the other force fields in AMBER, FF96 force field strongly favors the hairpin conformations.<sup>25–28</sup> On the other hand, by comparing REMD simulation results on the folding of polypeptide Ala10 with the GB solvent models to those with explicit TIP3P solvent model, Roe et al. observed that GB models over-stabilize  $\alpha$ -helical conformations.<sup>52</sup> Moreover, the solvent-accessible surface area (SASA) model, combining with the GB model and accounting for the nonpolar part of the salvation free energy, stabilizes the compact structures and thus artificially increases the transition temperature of the protein.<sup>53</sup> These factors, together, deviate the calculated melting temperatures from the experimentally determined data. Even so, compared to most of the previously reported melting temperatures in various MD simulations on the folding of the above-mentioned hairpins,<sup>4,20,53,54</sup> our results are within reasonable range.

Next we calculated the unfolding free energy as a function of temperature. To fit to the experiment condition, we performed the calculations in the temperature range of 270–380 K. We should note here that the melting temperature calculated using the free energy diagram depends on the definition of the folded structure (see the definition in Materials and Methods Section) and thus can deviate from that obtained from the heat capacity calculations in Figure 2. Figure 3a shows the free energy change for the transition of folded → unfolded state as a function of temperature. As seen from this figure, for peptide 1, TRPZIP2, and GB1, the error bars are rather small in the temperature range under study. For TRPZIP4, the error bars in the low temperature are apparently larger than the other three polypeptides. It is also seen from this figure that all four polypeptides are stable ( $\Delta G > 0$ ) in a rather large temperature range, including room temperature. For all polypeptides except TRPZIP4, only one transition temperature (at which  $\Delta G = 0$ ) is observed in the

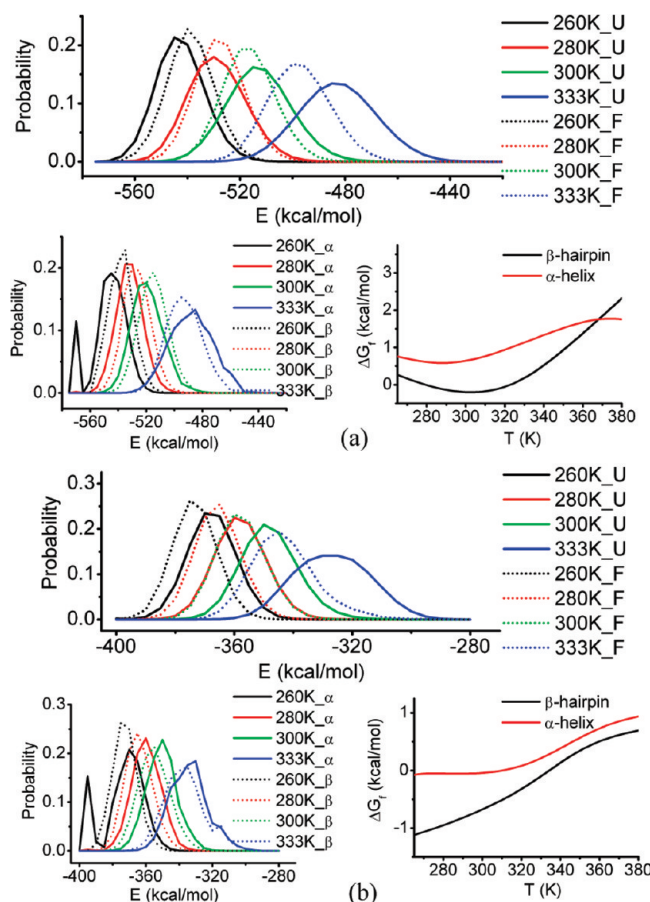


**Figure 4.** Comparison of unfolded (U) structures to folded (F) structures for (a) TRPZIP4 and (b) TRPZIP2 at different temperatures. Top: the potential energy distribution of the unfolded (solid lines) and folded structures (dash lines); left bottom: the potential energy distribution of  $\alpha$ -helix ( $\alpha$ , solid lines) and  $\beta$ -hairpin ( $\beta$ , dash lines); and right bottom: the temperature dependence of the unfolding free energy of  $\alpha$ -helix and  $\beta$ -hairpin.

entire temperature range studied. The native  $\beta$ -structure of TRPZIP4 becomes unstable at both low and high temperatures, while the other three polypeptides (especially TRPZIP2, the unfolding free energy of which increases with the decreasing temperature in the entire temperature range) have the native state as the stable structure at all low temperatures.

To further understand the structure stability as a function of temperature, we also calculated the distribution of potential energy for both folded and unfolded structures at various temperatures. (As mentioned earlier, the folded structures are defined as the ones with at least three backbone hydrogen bonds formed and the left structures with less than three hydrogen bonds formed refer to the unfolded structures.) Since TRPZIP4 and TRPZIP2 represent two extreme behaviors among the four systems, the results are only shown for these two polypeptides (see Figure 4a and b). It is shown in Figure 4a that at low temperatures, the potential energy of unfolded TRPZIP4 is lower than that of the folded structure. This result shows that the breaking of the TRPZIP4 native structure at low temperatures is mainly due to an enthalpy effect. [A cluster analysis of its non-native structures shows that as temperature decreases, the probability of

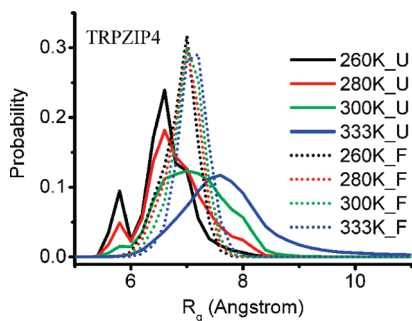


**Figure 5.** Radius gyration ( $R_g$ ) distribution of unfolded (U, solid lines) and folded (F, dash lines) structures of TRPZIP4 at different temperatures.

forming  $\alpha$ -helix increases for TRPZIP4 (see the comparison of the formation free energy of  $\alpha$ -helix to that of  $\beta$ -hairpin in Figure 4a). Due to the unstable turn of this polypeptide, the  $\alpha$ -helix indeed has lower energy than the  $\beta$ -hairpin structure (Figure 4a).] In contrast, the unfolded structures of TRPZIP4 at high temperatures and the unfolded structures of TRPZIP2 at both high and low temperatures (Figure 4b) are all of higher energies than their respective folded structures. Therefore, the unfolding of TRPZIP4 at high temperatures is primarily driven by the entropy increase. This entropic effect is also responsible for the heated denaturation of TRPZIP2. On the other hand, since the native  $\beta$ -structure has low energy (partly due to the very stable turn) and the unfolding enthalpy is positive, TRPZIP2 native structure becomes more stable as temperature decreases. Accordingly, the formation probability of  $\alpha$ -helix decreases as temperature decreases for TRPZIP2.

**Enthalpic versus Entropic Contributions in  $\beta$ -Structure Formation.** The unfolding enthalpy and entropy as functions of temperature are shown in Figure 3b and c, respectively. It is seen from these figures that the four polypeptides show dramatically different features. The most noticeable difference is again between TRPZIP4 and TRPZIP2, while peptide 1 and GB1 show behaviors in between. At low temperatures, the unfolding entropy is large and negative for TRPZIP4 and is large but positive for TRPZIP2. These values are small for GB1 (slightly negative) and peptide 1 (slightly positive and showing a minimum at  $\sim 300$  K). At high temperatures, the unfolding entropy is positive for all four polypeptides, with TRPZIP4 and peptide 1 having much larger values than the other two. These results again show that the breaking of the native structure of TRPZIP4 is enthalpically driven at low temperatures and entropically driven at high temperatures. Since the behavior of TRPZIP4 resembles a class of proteins which exhibit both cold and heated denaturation of native structures, we performed further analysis on its non-native structures at both low and high temperatures. It is seen from the radius gyration distribution function that the non-native structures are indeed more compact at low temperatures than those at higher temperatures (Figure 5). The former are more and the latter are less compact than the room temperature native structures.

## Temperature Dependence of the Folding Mechanism.

As discussed earlier, one way of distinguishing different folding mechanisms is to examine the formation order of the different structural elements: the hydrophobic core, the turn, and the hydrogen-bond assembly. We thus show in Figure 6 the free energy landscapes of the folding of the four polypeptides as a function of the collective coordinates, e.g., the number of backbone hydrogen bonds formed ( $N_{HB}$ ), the number of native hydrophobic contacts formed ( $N_{HC}$ ), and the root-mean-square displacement of the turn segment ( $rmsd_{turn}$ ) at different temperatures (273, 300, and 350 K). It is seen from these figures that the free energy profiles change with temperature in a similar way for all polypeptides. Although the folding pathways (as shown by the minimum free energy pathways, the dash lines in Figure 6a–d) of peptide 1 and TRPZIP2 are different from those of GB1 and TRPZIP4 at each temperature and the relative stability of the folded structures decrease with increasing temperature, the temperature dependence of the free energy profile shape is weak. In particular, the minimum free energy pathways only shift slightly for each polypeptide. These results show that the folding mechanisms of these polypeptides are largely determined by their sequences but are robust to the temperature change.

For GB1 and TRPZIP4 which possess a disfavored turn structure, the hydrophobic core formation is a barrierless process and thus is very easy to occur in the entire temperature range under study (see the free energy landscape as a function of  $N_{HC}$  and  $rmsd_{turn}$  in Figure 6c and d). The turn formation, however, constantly associates with a free energy barrier and remains as the rate-limiting step (the energy barrier for the hydrogen-bond formation is smaller than that of the turn formation as shown in the free energy landscape as the function of  $N_{HB}$  and  $rmsd_{turn}$  in Figure 6c and d).

On the other hand, in the folding of peptide 1 and TRPZIP2 which have the strongly favored turn structure, the hydrogen-bond formation is rate-limiting (see the free energy barrier in the free energy landscape as a function of  $N_{HB}$  and  $rmsd_{turn}$  in Figure 6a and b). Moreover, the single local minimum in the free energy landscape as a function of  $N_{HC}$  and  $rmsd_{turn}$  for peptide 1 shows that the turn formation is a barrierless process. The turn keeps stable once it is formed, whereas the hydrophobic interaction is weak. The turn structure of peptide 1 becomes unstable at the high temperature, as revealed by the broader local minimum in the same free energy landscape at the high temperature. The free energy landscape as a function of  $N_{HC}$  and  $rmsd_{turn}$  for TRPZIP2 at low and middle temperatures (273 and 300 K) has two local minima, corresponding to one state at which only a portion of hydrophobic interactions are formed and the turn is not and the other state at which both the hydrophobic core and the turn are formed. This shows that the hydrophobic core formation is facilitated by the turn formation in TRPZIP4. Therefore at any temperature, the difference of the side-chain hydrophobicity and particularly the turn stability changes the shape of the folding free energy landscapes and leads to the different folding mechanism of  $\beta$ -hairpins. Nevertheless the temperature only changes the

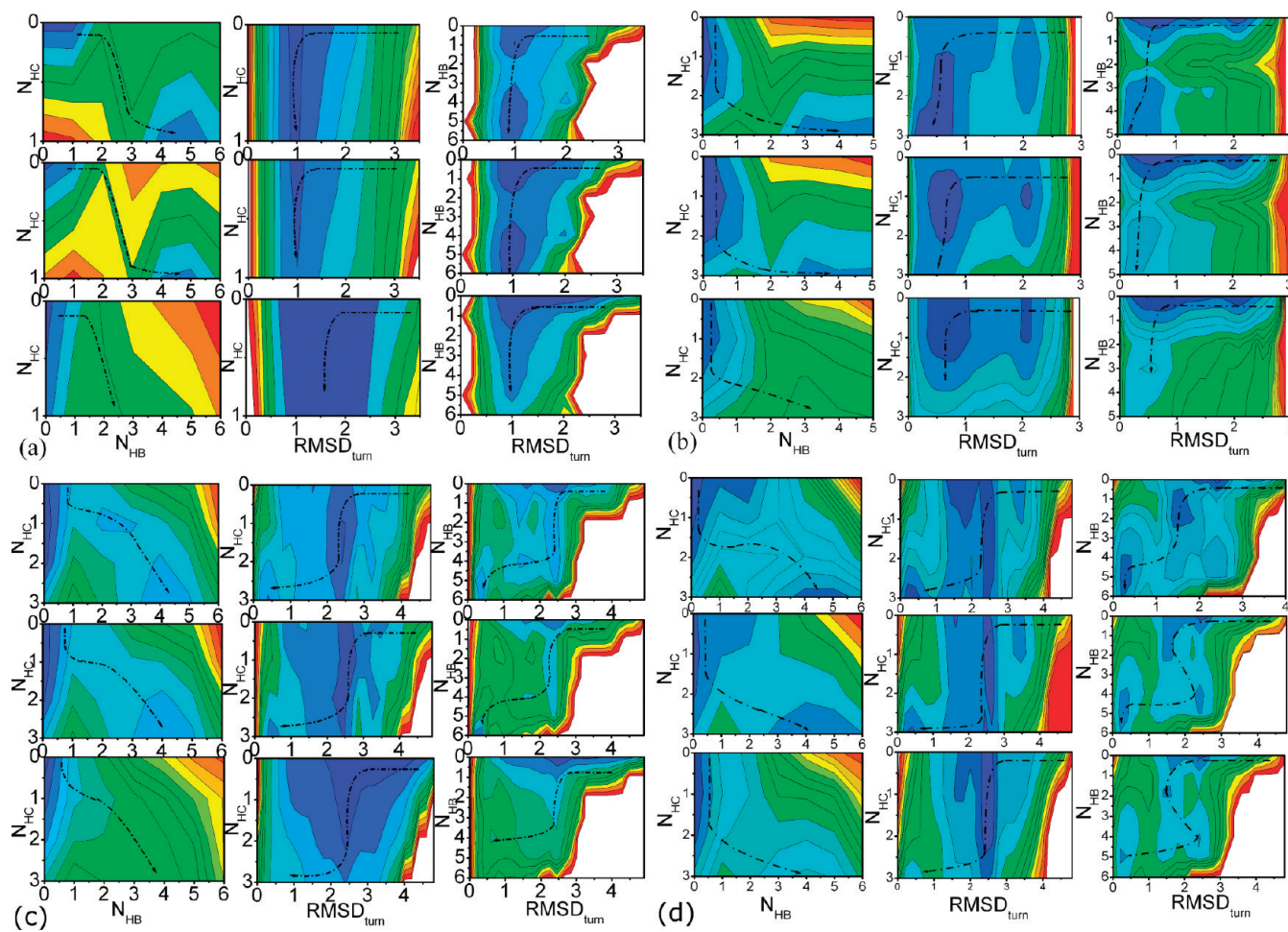


**Figure 6.** Free energy landscapes as a function of several collective coordinates including the number of backbone hydrogen bonds formed ( $N_{\text{HB}}$ ), the number of native hydrophobic contacts formed ( $N_{\text{HC}}$ ), and the root-mean-square displacement of the turn ( $\text{rmsd}_{\text{turn}}$ ) for (a) peptide 1, (b) TRPZIP2, (c) GB1, and (d) TRPZIP4 at different temperatures (in all figures (a–d), top panel: 273, middle panel: 300, and bottom panel: 350 K).

stability of a  $\beta$ -hairpin structure but not its folding pathway. These results might be thought to support the usage of high-temperature unfolding in understanding the protein folding mechanism at room temperature.

**Temperature Dependence of the Formation and Stability of Backbone Hydrogen Bonds.** One interesting question in understanding the  $\beta$ -structure formation is on the sequence of backbone hydrogen-bond formation (e.g., “zip-in” versus “zip-out”) and on its temperature dependence. To answer this question, we first calculated the average formation probabilities of individual hydrogen bonds for the four  $\beta$ -hairpins, and the results are shown in Figure 7(a–d). As demonstrated in these figures, the hydrogen-bond stability of the four polypeptides shows strong and different temperature dependence (each consistent with the corresponding free energy diagram shown in Figure 3a). In accordance with the high stability of their folded structures at low temperatures, the majority of the hydrogen bonds of GB1, peptide 1, and TRPZIP2 possess higher stabilities at lower temperatures, while the hydrogen bonds of TRPZIP4 are the most stable in the intermediate temperature region. There are also noticeable common features among the four polypeptides in the temperature dependence of their hydrogen-bond stability. For instance, it is seen from Figure 7 that the stability of

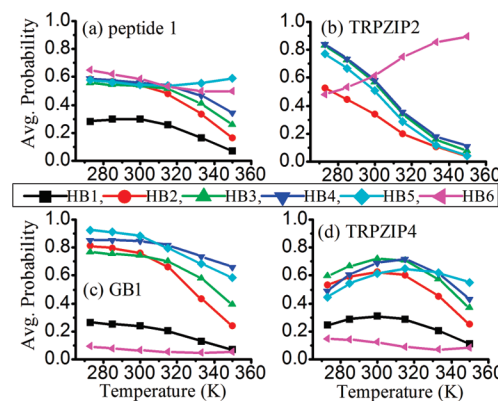


**Figure 7.** Average formation probability of individual backbone hydrogen bonds for (a) peptide 1, (b) TRPZIP2, (c) GB1, and (d) TRPZIP4 at different temperatures.

most inner hydrogen bonds (HB6 for GB1, TRPZIP2, and TRPZIP4 and HBs 5 and 6 for peptide 1) increases with temperature in the high-temperature range ( $>320$  K). The stability of the other hydrogen bonds, in particular the terminal ones, decreases with temperature in this temperature range. The reason behind the difference between inner and outer hydrogen bonds will be discussed later.

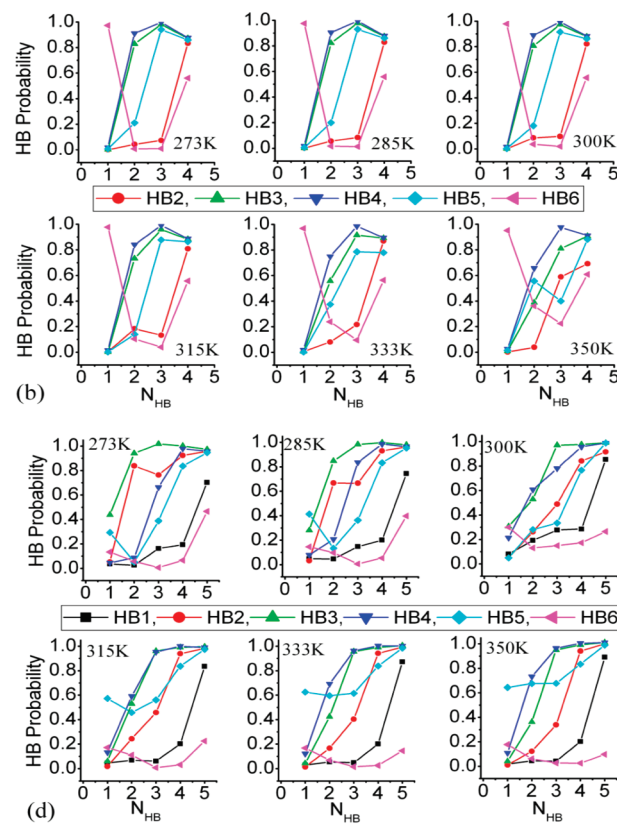
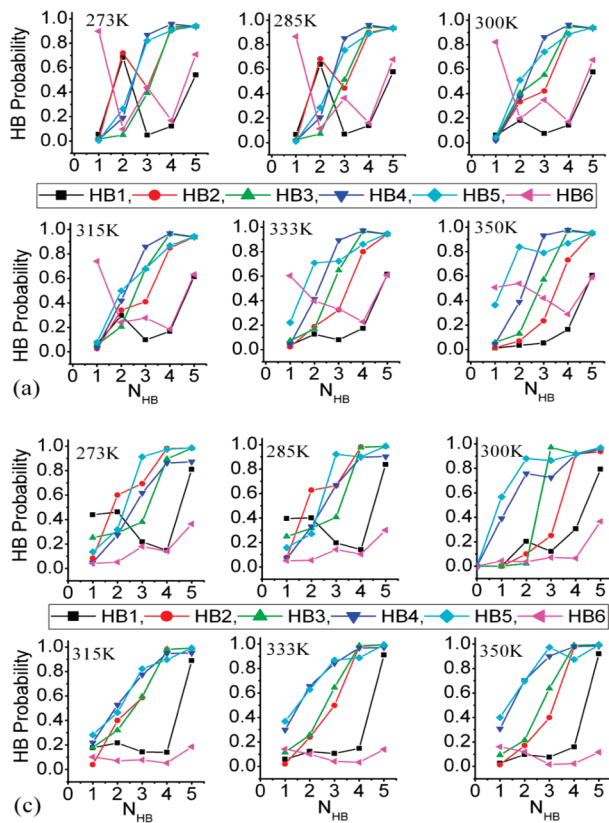


**Figure 8.** Formation probability of individual backbone hydrogen bonds as a function of the total number of formed hydrogen bonds for (a) peptide 1, (b) TRPZIP2, (c) GB1, and (d) TRPZIP4 at different temperatures.

In TRPZIP2, the stability of its hydrogen bonds except for the most inner one (HB6, whose stability increases with increasing temperature) markedly decreases with temperature. TRPZIP4, on the other hand, exhibits a maximum stability at the intermediate temperature range. Both its unfolding free energy (Figure 3a) and the formation probability of backbone hydrogen bonds, except for HB6, are bell-shaped. The temperatures at which individual hydrogen bonds show the highest stability increase systematically from the terminal (HB1 and HB2) to the inner positions. The stability of backbone hydrogen bonds of peptide 1 and GB1, the two polypeptides with weak hydrophobic core clusters, depends on temperature roughly in the same fashion. The main difference between peptide 1 and GB1 is in HB6, which is much more stable in peptide 1 than in GB1 as a result of the more stable turn in the former. Moreover, it appears that HB6 has an effect on the stability of the neighboring HB5, which also shows slightly different temperature dependence in peptide 1 and GB1. Overall, from the above analysis, one concludes that the increase of temperature in the high temperature region destabilizes terminal hydrogen bonds that are further away from the turn and either stabilizes or has little effect on the hydrogen bonds close to the turn. The decrease of temperature in the low temperature region appears to increase the relative stability of the terminal hydrogen bonds and either destabilizes or has little effect on the ones near the turn.

In addition to the temperature dependence of the average stability of hydrogen bonds shown in Figure 7, we also investigated the formation probability of each individual hydrogen bond in the assembling of backbone hydrogen

bonds during the formation of the native structure for each polypeptide. These data are shown in Figure 8 as a function of the total number of hydrogen bonds formed. The figure thus illuminates the stability and the formation order of backbone hydrogen bonds along the lowest free energy pathway in each polypeptide. The earlier the hydrogen bond appears in the high-formation probability region, the easier is it formed, namely the more preferential is its formation along the lowest free energy pathway in the assembling of backbone hydrogen bonds. As an example in Figure 8c, although the hydrogen-bond formation order of GB1 along the lowest free energy pathway is roughly 1 → 2 → 3, 4, 5 → 6 at low temperatures (the formation of HB6 is difficult due to the unstable turn of GB1; HB1 forms easily in the folding process, whereas becomes broken again during the assembling of the hydrogen bonds in the middle position), it roughly converts to the “zip-out” mechanism at high temperatures (5, 4 → 3 → 2 → 1 → 6). A similar temperature dependence of hydrogen-bond formation order along the lowest free energy pathway is also observed for the other three polypeptides. As shown in Figure 8a, at low temperatures, the appearance order of hydrogen bonds (from high to low probabilities) of peptide 1 is roughly 6 → 1, 2 → 4, 5 → 3 (HB6 forms easily as a result of the stable turn of peptide 1 but breaks down during the rest of the structure formation process). As temperature increases, the formation of terminal hydrogen bonds becomes more difficult, and at temperatures higher than 300 K, the formation order of hydrogen bonds along the lowest free energy pathway is 6 → 5 → 4 → 3 → 2 → 1, corresponding to a “zip-out” mechanism.

**Table 1.** Native Backbone Hydrogen Bonds along the Strands and Hydrogen Bonds within the Turn Region in GB1 and TRPZIP4 Polypeptides

backbone HBs		HBs in the turn region	
HB1	T15O-E2H	HBt1	D6O $\delta$ -T9H $\gamma$ 1
HB2	E2O-T15H	HBt2	T9O $\gamma$ 1-T11H $\gamma$ 1
HB3	T13O-T4H	HBt3	D6O $\delta$ -T9H
HB4	T4O-T13H	HBt4	D6O-K10H
HB5	T11O-D6H	HBt5	D6O $\delta$ -A8H
HB6	D6O-T11H	HBt6	D7O-K10H

TRPZIP2 and TRPZIP4 both possess a strong hydrophobic core that is close to the center of strands. As a result of the strong hydrophobic packing of these residues, the formation of hydrogen bonds in the middle of strands (HBs 2–4) is strongly favored compared to those in GB1 and peptide 1. Consistent with the facilitated hydrogen-bond formation in the middle, at low temperatures the hydrogen-bond formation along the lowest free energy pathway initiates from the middle of strands for both TRPZIP2 and TRPZIP4 (see the high formation probability of H3 and H4 in Figure 8b and d). For TRPZIP4, as temperature increases, the stability of the inner hydrogen bonds increases over the terminal ones as discussed earlier, and as a result, the formation of hydrogen bonds along the lowest free energy pathway follows a “zip-out” mechanism at high temperatures ( $5 \rightarrow 4 \rightarrow 3 \rightarrow 2 \rightarrow 1$ , HB6 is unstable due to the unstable turn structure of TRPZIP4). For TRPZIP2, at low temperatures, along the lowest free energy pathway, the formation of HB3 is easier than HB5, and at high temperatures a reverse order is seen, although in all temperatures HB4 appears to be the most easily formed. At all temperatures, the inner hydrogen bond HB6 forms easily as a result of the stable turn of TRPZIP2. However, only at high temperatures, it remains relatively stable during the assembling of the rest hydrogen bonds, again supporting a transition toward the “zip-out” mechanism.

**Temperature Dependence of the Formation and Stability of Hydrogen Bonds in the Turn Region.** Different from the type I' turn in peptide 1 and TRPZIP2, the type I turn in GB1 and TRPZIP4 possesses a hydrogen-bond network covering the backbone and side chains of the turn residues (Asp6–Thr11),<sup>24</sup> as organized in Table 1 (HBt1–6) and shown in Figure 9. In addition, a salt bridge is formed between Asp7 and Lys10 side chains. As demonstrated by several novel experiments,<sup>44,55</sup> the hydrogen bonds in the turn region, particularly those formed between Asp6 and other residues, are crucial to the stability of the turn structure and the folding rate of GB1 and TRPZIP4. For instance, the T-jump IR experiment by Du et al. showed that the replacement of Asp6 by alanine decreases the folding rate of TRPZIP4 by ~9 times, whereas the mutation of Asp7 by alanine only decreases the folding rate of the same polypeptide slightly.<sup>44</sup> Moreover, the NMR stability experiment on GB1 peptide demonstrated that the mutating of either Asp6, Lys10, or Thr9 with alanine destabilizes the turn structure, and the destabilization degree follows the order of Asp6>Lys10>Thr9.<sup>55</sup>

We calculated the average formation probabilities of individual hydrogen bonds in the turn region of GB1 and

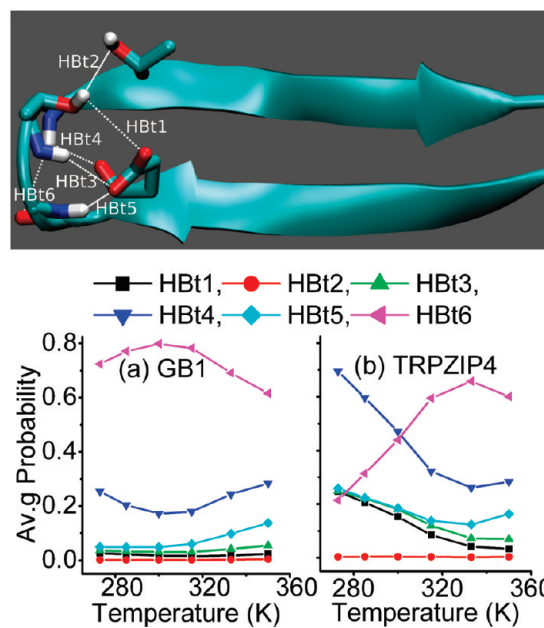


**Figure 9.** Average formation probability of individual hydrogen bonds in the turn region of (a) GB1 and (b) TRPZIP4. The top panel is the schematic representation of the hydrogen-bond network in GB1 peptide.

TRPZIP4, respectively, and the results are shown in Figure 9. As shown in this figure, the only two hydrogen bonds formed between the backbones in the turn region, HBt4 (D7O–K10H) and HBt6 (D7O–K10H), show much higher stabilities than other hydrogen bonds in both GB1 and TRPZIP4. Interestingly, these two hydrogen bonds have the totally opposite temperature dependence on their stability. On the contrary, Hbt2 formed between the side chains of Thr9 and Thr11 always has the extremely low stability in the whole temperature range under study. The left three hydrogen bonds (HBt1, HBt3, and HBt5), which are formed between the side chain of Asp6 and either backbone or side chain of other residues, have the middle stability, especially in TRPZIP4. Since HBt2 contributes least to the hydrogen-bond network in the turn region, the T9A mutation should lead to a minor change in the turn structure stability. On the other hand, the D7A or K10A mutation results in the cancellation of the salt bridge. Nevertheless, this side-chain configuration change will not largely affect the stability of the backbone–backbone hydrogen bonds. The D6A mutation, however, removes the three hydrogen bonds of HBt1, HBt3, and HBt5 which have the middle stability in the hydrogen-bond network in the turn region. As a result, only the D6A mutation will largely decrease the turn structure stability, which is consistent with the experimental observations mentioned above.<sup>44,55</sup>

## Conclusions

In this article, we performed detailed thermodynamics study on the temperature dependence in the folding of several polypeptides that form stable  $\beta$ -hairpin structures. The current study is expected to provide a qualitative understanding of the folding mechanism of  $\beta$ -hairpin structures and a fully atomic description of the structure formation process (par-

ticularly the backbone hydrogen-bond formation) for various amino acid sequences at different temperatures. Simulations were performed using an implicit solvent model, which was proven to yield free energy profiles in reasonable agreement with those obtained using explicit solvent models.<sup>34</sup> Cautions, however, have to be exercised in quantitative interpretation of the simulation data. For example, it will not be surprising that water contributes significantly (if not dominantly) to the folding energy of protein. Although the effects of water to the free energy were considered in a continuum model, there is no guarantee that the effects have been taken into account faithfully. Therefore, the current study should be understood in a more qualitative way. It provides a useful model system for the understanding of protein sequence and temperature dependence of protein folding mechanism. The results of the very recent isotope-edited two-dimensional infrared spectroscopy experiment on the temperature dependence of the backbone hydrogen-bond stability of TRPZIP2,<sup>46</sup> which are consistent with our predictions, demonstrate the validity of the present methodology in exploring the folding mechanism of  $\beta$ -hairpins.

Four polypeptides (peptide 1, TRPZIP2, GB1, and TRPZIP4), which differ at their side-chain hydrophobicity and turn stability, were used as the model systems in the present study. Based on the analysis of a variety of thermodynamics data, we showed that the folding of simple  $\beta$ -hairpin structures is highly sequence and temperature dependent. First, the formation order of the three important structural elements along the minimum free energy pathway in the free energy landscapes appears to be only sequence dependent and to be largely unaffected by the temperature change between 270 to 380 K (see Figure 6). The presence of the strong  $\beta$ -turn-promoting sequence in peptide 1 and TRPZIP2 leads to the folding of  $\beta$ -hairpins following the modified “hydrogen-bond centric” mechanism.<sup>19</sup> On the contrary, the presence of disfavored turn structure in GB1 and TRPZIP4 makes the hairpin folding more consistent with the “hydrophobic core centric” mechanism. Second, both the hydrophobic core cluster and the turn affect the nearby hydrogen bonds. The favored turn structure assists the formation of the inner hydrogen bond (HB6), whereas the strong hydrophobic core cluster strengthens the stability of hydrogen bonds (HBs 3 and 4) in the middle of strands. These effects lead to the different stability and formation order of individual hydrogen bonds at a given temperature. Finally, the pathway for the formation of backbone hydrogen bonds shows a strong dependence on temperature. At low temperatures, the formation of hydrogen bonds is likely initiated from the middle of the strands (at very low temperatures the formation of the terminal hydrogen bonds also become largely favored, but the terminal hydrogen bonds tend to be broken during the assembling of the rest hydrogen bonds, see the examples of GB1 and peptide 1 in Figure 8a and c, respectively). At high temperatures, however, there is a strong tendency for the hydrogen-bond assembling to be initiated from the turn position and to propagate through a “zip-out” mechanism. These results are easily understood in terms of entropy and enthalpy contributions in hydrogen-bond formation.

Without considering the side-chain interactions, it is easy to see that the breaking of terminal hydrogen bonds increases the configuration entropy to a larger extent than the breaking of inner hydrogen bonds does, simply because of their larger separation along the amino acid chain. As a result, one expects that under these hypothetical conditions, the formation of the terminal hydrogen bonds is less favored compared to the inner ones at high temperatures. At high temperatures, since the denatured states also likely have interrupted side-chain interactions, it is thus conceivable that the entropy effects mentioned above dominate the formation probability of the individual hydrogen bonds, and as a result, the stability of the hydrogen bonds increases from the turn to the terminal position, as observed in Figure 7.

At lower temperatures, the enthalpy effects also play important roles, and as a result, the hydrogen-bond stability is strongly affected by their local interactions, the simple order observed at high temperatures therefore disappears. In contrast, the hydrophobic cluster near the hydrogen bonds tends to shield them from solvent attack and effectively creates a low-dielectric environment. As a result, these hydrogen bonds can be expected to be more stable. This stabilization of the hydrogen bonds through this enthalpic effect is most easily seen from the hydrogen-bond stability of TRPZIP2 and TRPZIP4 at low temperatures. It is of great interest for the numerous predictions made through this study, for example, those on the temperature dependence of hydrogen-bond stability and those on the compactness of non-native states (see Figure 5), to be tested by experiments.

**Acknowledgment.** This study was supported financially by Peking University. We thank Professor Andrei Tokmakoff for discussions. Y.Q.G. is a 2008 Changjiang Scholar. Q.S. thanks China Postdoctoral Science Foundation funded project.

## References

- (1) Galzitskaya, O. V. *Mol. Biol.* **2002**, *36*, 607–612.
- (2) Hughes, R. M.; Waters, M. L. *Curr. Opin. Struct. Biol.* **2006**, *16*, 514–524.
- (3) Zhou, R. H.; Berne, B. J. *Proc. Natl. Acad. Sci. U.S.A.* **2002**, *99*, 12777–12782.
- (4) Zhou, R. H.; Berne, B. J.; Germain, R. *Proc. Natl. Acad. Sci. U.S.A.* **2001**, *98*, 14931–14936.
- (5) Schaefer, M.; Bartels, C.; Karplus, M. *J. Mol. Biol.* **1998**, *284*, 835–848.
- (6) Dinner, A. R.; Lazaridis, T.; Karplus, M. *Proc. Natl. Acad. Sci. U.S.A.* **1999**, *96*, 9068–9073.
- (7) Blanco, F. J.; Jimenez, M. A.; Pineda, A.; Rico, M.; Santoro, J.; Nieto, J. L. *Biochemistry* **1994**, *33*, 6004–6014.
- (8) Blanco, F. J.; Rivas, G.; Serrano, L. *Nat. Struct. Biol.* **1994**, *1*, 584–590.
- (9) Bonvin, A. M. J. J.; van Gunsteren, W. F. *J. Mol. Biol.* **2000**, *296*, 255–268.
- (10) Munoz, V.; Thompson, P. A.; Hofrichter, J.; Eaton, W. A. *Nature* **1997**, *390*, 196–199.
- (11) Cochran, A. G.; Skelton, N. J.; Starovasnik, M. A. *Proc. Natl. Acad. Sci. U.S.A.* **2001**, *98*, 5578–5583.

- (12) Searle, M. S.; Ciani, B. *Curr. Opin. Struct. Biol.* **2004**, *14*, 458–464.
- (13) Searle, M. S.; Zerella, R.; Dudley, D. H.; Packman, L. C. *Protein Eng.* **1996**, *9*, 559–565.
- (14) Zerella, R.; Evans, P. A.; Ionides, J. M. C.; Packman, L. C.; Trotter, B. W.; Mackay, J. P.; Williams, D. H. *Protein Sci.* **1999**, *8*, 1320–1331.
- (15) Espinosa, J. F.; Munoz, V.; Gellman, S. H. *J. Mol. Biol.* **2001**, *306*, 397–402.
- (16) Munoz, V.; Henry, E. R.; Hofrichter, J.; Eaton, W. A. *Proc. Natl. Acad. Sci. U.S.A.* **1998**, *95*, 5872–5879.
- (17) Silva, R. A. G. D.; Sherman, S. A.; Keiderling, T. A. *Biopolymers* **1999**, *50*, 413–423.
- (18) Kolinski, A.; Ilkowski, B.; Skolnick, J. *Biophys. J.* **1999**, *77*, 2942–2952.
- (19) Tsai, J.; Levitt, M. *Biophys. Chem.* **2002**, *101*, 187–201.
- (20) Garcia, A. E.; Sanbonmatsu, K. Y. *Proteins* **2001**, *42*, 345–354.
- (21) Pande, V. S.; Rokhsar, D. S. *Proc. Natl. Acad. Sci. U.S.A.* **1999**, *96*, 9062–9067.
- (22) Nguyen, P. H.; Stock, G.; Mittag, E.; Hu, C. K.; Li, M. S. *Proteins* **2005**, *61*, 795–808.
- (23) Wei, G. H.; Mousseau, N.; Derreumaux, P. *Proteins* **2004**, *56*, 464–474.
- (24) Yoda, T.; Sugita, Y.; Okamoto, Y. *Proteins* **2007**, *66*, 846–859.
- (25) Ono, S.; Nakajima, N.; Higo, J.; Nakamura, H. *J. Comput. Chem.* **2000**, *21*, 748–762.
- (26) Zaman, M. H.; Shen, M. Y.; Berry, R. S.; Freed, K. F.; Sosnick, T. R. *J. Mol. Biol.* **2003**, *331*, 693–711.
- (27) Higo, J.; Ito, N.; Kuroda, M.; Ono, S.; Nakajima, N.; Nakamura, H. *Protein Sci.* **2001**, *10*, 1160–1171.
- (28) Kamiya, N.; Higo, J.; Nakamura, H. *Protein Sci.* **2002**, *11*, 2297–2307.
- (29) Qiu, D.; Shenkin, P. S.; Hollinger, F. P.; Still, W. C. *J. Phys. Chem. A* **1997**, *101*, 3005–3014.
- (30) Zhou, R. H. *Proteins* **2003**, *53*, 148–161.
- (31) Shell, M. S.; Ritterson, R.; Dill, K. A. *J. Phys. Chem. B* **2008**, *112*, 6878–6886.
- (32) Onufriev, A.; Bashford, D.; Case, D. A. *Proteins* **2004**, *55*, 383–394.
- (33) Mongan, J.; Simmerling, C.; McCammon, J. A.; Case, D. A.; Onufriev, A. *J. Chem. Theory Comput.* **2007**, *3*, 156–169.
- (34) Shao, Q.; Yang, L. J.; Gao, Y. Q. *J. Chem. Phys.* **2009**, *130*, 195104/1–195104/6.
- (35) Ozkan, S. B.; Wu, G. A.; Chodera, J. D.; Dill, K. A. *Proc. Natl. Acad. Sci. U.S.A.* **2007**, *104*, 11987–11992.
- (36) Gao, Y. Q. *J. Chem. Phys.* **2008**, *128*, 064105/1–064105/5.
- (37) Gao, Y. Q.; Yang, L. J. *J. Chem. Phys.* **2006**, *125*, 114103/1–114103/5.
- (38) Shao, Q.; Wei, H. Y.; Gao, Y. Q. *J. Mol. Biol.* **2010**, *402*, 595–609.
- (39) Cornell, W. D.; Cieplak, P.; Bayly, C. I.; Gould, I. R.; Merz, K. M.; Ferguson, D. M.; Spellmeyer, D. C.; Fox, T.; Caldwell, J. W.; Kollman, P. A. *J. Am. Chem. Soc.* **1995**, *117*, 5179–5197.
- (40) Santiveri, C. M.; Pantoja-Uceda, D.; Rico, M.; Jimenez, M. A. *Biopolymers* **2005**, *79*, 150–162.
- (41) Gronenborn, A. M.; Clore, G. M. *Science* **1991**, *254*, 581–582.
- (42) Santiveri, C. M.; Santoro, J.; Rico, M.; Jimenez, M. A. *J. Am. Chem. Soc.* **2002**, *124*, 14903–14909.
- (43) Du, D. G.; Zhu, Y. J.; Huang, C. Y.; Gai, F. *Proc. Natl. Acad. Sci. U.S.A.* **2004**, *101*, 15915–15920.
- (44) Du, D. G.; Tucker, M. J.; Gai, F. *Biochemistry* **2006**, *45*, 2668–2678.
- (45) Yang, L. J.; Shao, Q.; Gao, Y. Q. *J. Phys. Chem. B* **2009**, *113*, 803–808.
- (46) Smith, W. A.; Lessing, J.; Ganim, Z.; Peng, C. S.; Tokmakoff, A. *J. Phys. Chem. B* **2010**, *114*, 10913–10924.
- (47) Ryckaert, J. P.; Ciccotti, G.; Berendsen, H. J. C. *J. Comput. Phys.* **1977**, *23*, 327–341.
- (48) Yang, L. J.; Shao, Q.; Gao, Y. Q. *J. Chem. Phys.* **2009**, *130*, 124111/1–124111/8.
- (49) Fesinmeyer, R. M.; Hudson, F. M.; Andersen, N. H. *J. Am. Chem. Soc.* **2004**, *126*, 7238–7243.
- (50) Olsen, K. A.; Fesinmeyer, R. M.; Stewart, J. M.; Andersen, N. H. *Proc. Natl. Acad. Sci. U.S.A.* **2005**, *102*, 15483–15487.
- (51) Huyghues-Despointes, B. M. P.; Qu, X. T.; Tsai, J.; Scholtz, J. M. *Proteins* **2006**, *63*, 1005–1017.
- (52) Roe, D. R.; Okur, A.; Wickstrom, L.; Hornak, V.; Simmerling, C. *J. Phys. Chem. B* **2007**, *111*, 1846–1857.
- (53) Hayer, N. R.; Singh, R. R. P.; Cox, D. L. arXiv:1009.0303v1 [q-bio.BM] published online: September 1, 2010.
- (54) Nymeyer, H. *J. Phys. Chem. B* **2009**, *113*, 8288–8295.
- (55) Kobayashi, N.; Honda, S.; Yoshii, H.; Munekata, E. *Biochemistry* **2000**, *39*, 6564–6571.

CT100436R